Article

Adsorption Properties of Diatomite Minerals on Glyceryl Monostearate for Antifogging of the Plastic Film

Jindi Zha, Hong Zhang,* Zhixiao Ren, Na Zhang, Gengdi Zheng, Wei Jin, and Jinsheng Liang*
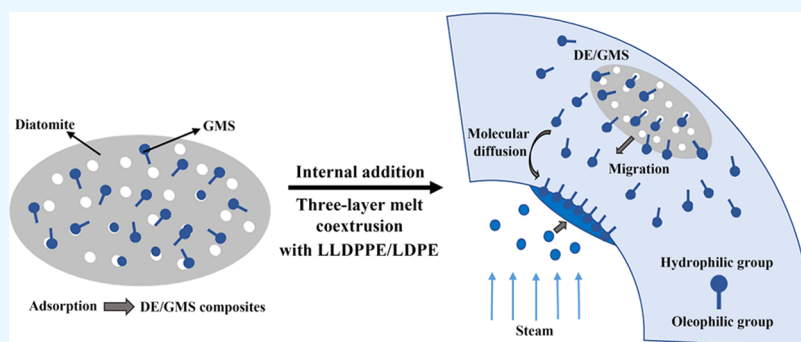
Read Online

ACCESS | Metrics & More | Article Recommendations | Supporting Information

ABSTRACT: Adding an appropriate amount and the stable precipitation of surfactant on the inner surface of agricultural plastic greenhouse films can prevent the formation of water droplets on the inner surface of the film to reduce its harmful effects in the process of plant cultivation and production. In this work, for the stable precipitation of the surfactant glycerol monostearate, diatomite minerals from three origins in China were compared through structural analysis and adsorption performance. The effects of acid treatments and alkali treatments on the mineral structure were studied, and the adsorption mechanism of glycerol monostearate was further investigated. The results show that the structural characteristics of Jilin diatomite are more suitable as adsorbents for glyceryl monostearate adsorption. Because diatomite is resistant to acids but not alkalis, when diatomite is treated with an alkali, impurities on its surface can be removed and the hydroxyl group and specific surface area can be greatly increased. The adsorption capacity of glycerol stearate was increased to 218.4 mg/g, or 32.08%, over its pretreatment level. The results show that this is mainly the result of physical adsorption caused by van der Waals force imbalance and chemisorption caused by a small number of hydrogen bonds. In addition, the dripping performance of this composite dripping film with mineral diatomite was better than that of the commercial dripping film, which provided a theoretical basis for efficient mineral slow-release drip irrigation composite film.

1. INTRODUCTION

With the rapid development of modern agriculture, greenhouse cultivation technology with plastic film has been widely used in China.[1,2] Among these films, polyethylene (PE) film is often used as a covering in greenhouses because of its better heat preservation and light transmission, which is hydrophobic thermoplastic. Within a greenhouse, temperature and humidity are usually higher than those outside, and water droplets may appear on the inner surface of PE film, which affects the quality and yield of the plants.[3−6] It was shown that surface condensation can be reduced by improving the film hydrophilicity.[7,8] Currently, methods for improving the hydrophilicity of PE film mainly include external coating and internal addition.[9,10] The internal addition method involves the addition of dripping agents, such as glycerol monostearate, Span 60, and Tween 80,[11−13] to the polyethylene substrate before extrusion or molding. A typical surfactant with lipophilic and hydrophilic polar groups, glycerol monostearate exhibits

good lubricity, emulsification, and surface activity. As a result, the most crucial ingredient in many of the commercial dripping agents for plastic films available on the market is glyceryl monostearate. The more hydrophilic the dripping agent, the less compatible it is with the resin, resulting in these small molecules continuously migrating to the inner surface of the membrane to form a hydrophilic film with water droplets,[14,15] and the dripper that migrates to the inner surface of the membrane is washed away by the water droplets. This results in a concentration gradient between the surface and inside, driving the agents to continuously migrate to the inner surface
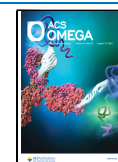
to maintain hydrophilicity, which eventually causes the film to gradually lose its dripping properties. Therefore, it is necessary to slow the migration of the dripping agent molecules and extend the drip time of the film.

In recent years, many strategies have been developed to delay the migration of the dripping agents. Among them, because the inorganic material can have good compatibility with the resin matrix, and there are many polar groups similar to hydroxyl groups on its surface, the precipitation of the dripping agent can be delayed by adsorption, surface grafting, and so on. Rosen-Kligvasser et al.[15] grafted glycerol monooleate onto the surface of silica particles, and the results of tests showed that silica particles could significantly slow down the migration rate. Yang et al.[16] synthesized a reactive type of agent, 18-alkyl diethanolamine acrylic monoester (EDM), which was grafted onto layered double hydroxides (LDHs) to retard migration. Zhu et al.[17] grafted diethanol-amine acrylate (AAM) onto the surface of kaolin and extruded with linear low-density polyethylene. The results showed that the accelerated falloff time of the composite film at 60 °C was 4 days longer than that of the ungrafted one. Natural minerals, as traditional inorganic materials, contain a variety of inorganic particles within them, and their unique structural properties endow them with excellent surface functionality, which can be used as carriers for slow-release droplets. In addition, they have the advantages of good humidity regulation, thermal stability, electrical insulation, and low infrared light transmittance, so they can not only fulfill their proper performance but also improve the air permeability and moisture permeability inside the film, as well as increase the effect of heat insulation and heat preservation.[18]

As a typical mineral material, diatomite provides physical active sites for adsorption due to its high permeability, low density, high specific surface area, and a large number of silicon hydroxyl groups. In addition, diatomite also has the characteristics of nontoxic, strong acid resistance, renewable, and low cost. Therefore, diatomite is a promising adsorption material.[19] It is often used to adsorb heavy metal ions, organic pollutants, and sustained-release drugs. Caliskan et al.[20] studied the factors of Zn(II) adsorption capacity of diatomite. It shows that the surface of diatomite with a high negative charge is beneficial to the adsorption of metal cations. In addition, pH is also a factor affecting the adsorption capacity of diatomite to Zn(II). When pH < 7.5, Zn(II) is mainly removed by adsorption. At pH 7.58, in addition to adsorption, some Zn(II) is converted into Zn(OH)$_2$, which increases the removal rate of Zn(II). Losic et al.[21] demonstrated for the first time the effectiveness of diatomite in drug delivery applications, which can load 22% hydrophobic small molecule indomethacin. Due to the surface micropores and internal hollow structure, the drug can be slowly and continuously released for more than 2 weeks after adsorption on the surface of diatomite. Aivalito et al.[22] studied the removal of benzene, toluene, ethylbenzene, m,p,o-xylene (BTEX), methyl tert-butyl ether (MTBE), and tert-amyl methyl ether (TAME) in aqueous solution by diatomite ore, heat treatment, chemical treatment, and chemical-heat treatment, respectively. The results showed that diatomite had a good adsorption effect on BTEX, MTBE, and TAME in aqueous solution. The adsorption capacity and equilibrium time of diatomite treated with HCl were the best, and the kinetic data fit well with the quasi-second-order model. The isothermal experimental data conformed with the Freundlich model.

In addition, some scholars have found that diatomite has the effect of delaying the precipitation of the dripping agent. He et al.[23] prepared microdiatomite-modified LDPE antifog film by blow molding method and studied the antifog performance and mechanical properties of the film. The results show that the film modified by inorganic micron diatomite with surface treatment agent has a more obvious antifog effect than that modified by antifog agent alone. Jingmei et al.[24] made a comparative study on the effects of inorganic powders such as white carbon black, diatomite, mica, and talc powder added to the drip film as sustained-release agents on the properties of the film. The results show that under the same conditions, the film with diatomite as the sustained-release agent has the longest duration, and compared with the other three powders with lamellar structure, the special porous structure of diatomite is easier to form pores, which is conducive to a series of behaviors such as adsorption, desorption, and migration of the droplets. However, the pore structure and surface properties of diatomite will affect the adsorption and sustained-release performance of nonionic surfactants. The morphological and structural qualities of raw diatomite from different origins vary depending on the aging and geographical conditions, and the adsorption properties can be significantly limited by the presence of contaminants and physicochemical structural defects in the raw mineral.[25,26] Thus, the secret to creating slow-release surfactant mineral composites is to choose the best diatomite for adsorption and optimize adsorption performance through treatment.

This work aims to prepare mineral composites with a high content of glycerol monostearate using the excellent physical adsorption properties of diatomite. The structural and adsorption properties of diatomites from different origins were optimized. Thus, the optimized sample was treated with acid and alkali, which modulated the surface properties and adsorption performance of glycerol monostearate. The adsorption mechanism of diatomite for surfactants was further analyzed, and the relationship between the minerals and dropping agents was discussed. In addition, the diatomite adsorbed with glycerol monostearate was used to prepare the composite drip film, and the main properties were tested, which laid the experimental foundation for future scale-up tests and application.

2. MATERIALS AND METHODS

2.1. Materials. The three diatomite samples used in the experiment were purchased from Hongxi Tai Chemical Co., Ltd. (Tianjin, China), which were from Hebei Province, Jilin Province, and the Inner Mongolia Autonomous Region (China). The samples had a particle size of about 10 μm, which were denoted as HB-DE, A-DE, and N-DE according to their locations. Glycerol monostearate (C$_{21}$H$_{42}$O$_4$, GMS, 99%) was purchased from Aladdin Biochemical Technology (Shanghai, China), and its chemical structure is shown in Figure 1. The other reagents used in this study were anhydrous ethanol (C$_2$H$_6$O, 99%), HCl (20 wt %), and NaOH (5 wt %). All reagents were used as received without further purification.

2.2. Treatment of the Diatomite Samples. The diatomite was treated with acid and alkali, respectively. An aqueous solution of sulfuric acid with a concentration of 23.7 wt % was added to a beaker containing diatomite at a solid−liquid ratio of 3:1. The mixture was then heated and stirred in a water bath at 75 °C for 10 h, followed by rinsing to neutralize, drying, and grinding. The resulting samples were
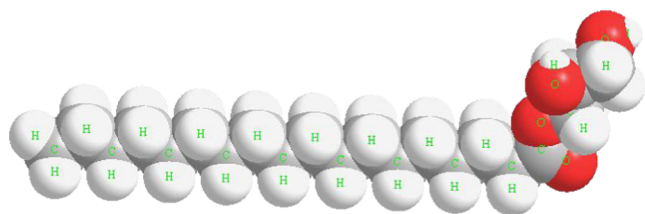
Figure 1. Molecular structure of the GMS.

named S-DE. Sodium hydroxide aqueous solution with a concentration of 5 (wt %) was added to the beaker with the diatomite at a solid−liquid ratio of 3:1, heated, and stirred in a water bath at 100 °C for 2 h, then rinsed to neutral, dried, and ground, and named as J-DE.

2.3. Preparation of LLDPE/LDPE-DE/GMS. The appropriate amount of feedstock resin LLDPE, LDPE, and 30.7 g of mineral dripping composite were mixed at high speed for 2 min in the GRH-10Z mixer. After thorough mixing, the mixture was placed in a YB-35L horizontal mixer for plasticizing. The SJ-90/30 screw extruder was used for extrusion, wire drawing, water cooling, and granulation to obtain 67.4 g of drip masterbatch for use. In this process, the mixer temperature was set to 140−160 °C, the plasticizing time was 15−20 min, and the single-screw granulator temperature was 110−150 °C.

2.4. Preparation of Dripping Film. The films were prepared by three-layer coextrusion LLDPE-DE/GMS and LDPE-DE/GMS with LLDPE or LDPE using an SJ60−1100 corotating twin-screw extruder. And this resulting sample was named L1. The inside of the extruder has a twin screw with a length-to-diameter ratio (L/D) of 44. The extrusion temperature was set at 150−200 °C from the feeder to the die. Sample films (thickness of 0.10 mm) were blown by using a single-screw extruder (L/D = 20) connected to a round die operating at 190 °C.

2.5. Characterization. XRD patterns of diatomite samples were collected using an X-ray diffractometer (Rigaku SmartLab 9KW, Japan) with Cu Kα radiation (λ = 0.15406 nm) from a diffraction angle of 10−90°. The microstructure was observed by scanning electron microscopy (SEM, Nova Nano SEM450, FEI). Fourier transform infrared spectroscopy (FTIR, Bruker V80, Germany) in the range of 4000−400 cm^{-1} was used to record the spectra of functional groups on the surface. Nitrogen adsorption−desorption isotherms were measured with Autosorb iQ2 (Quatachrome, USA) at −196 °C. The specific surface area was determined from the isotherms by the Brunauer−Emmet−Teller (BET) method, and the pore size distributions were calculated by the Barrett−Joyner−Halenda (BJH) method using the nitrogen adsorption branch of the isotherms. Contact angles were measured by an OCA 30 Droplet Shape Analyzer. The sample of the film was on a drip shape analyzer sample stage. 2 μL of deionized water was placed on the sample film, and the angle was recorded within 5 s and the image was saved. The film was measured 5 times at different positions, and the average value was taken as the test result. The dripping time of films was investigated by a DP-D80 Type Accelerated Dripping Tester at 60 °C. Water was added regularly to ensure that the water level and temperature did not fluctuate considerably. Condensation on the inner surface of films was observed, defining the dripping performance loss when 30% of the inner surface of the film is covered by water droplets.

2.6. Adsorption Experiment. The batch adsorption experiments were performed on a gas bath thermostat shaker model ZD-85 (Tianjin Sedlis Experimental Analytical Instrument Manufacturing Plant) at 170 rpm. First, 5 g of GMS pellets were placed in an appropriate amount of anhydrous ethanol to prepare the solution in the concentration range of 20−100 g/L. A 5 g portion of raw and treated diatomite samples were, respectively, added to the prepared solutions of different concentrations of GMS at room temperature for the experiments. After the adsorption, the suspension was centrifuged at 10,000 rpm for 10 min, and the filter residue of the DE/GMS composites was collected and dried at 40 °C to a constant weight. The dried composites were further used for characterization. The raw diatomite was named HB-DE/GMS, A-DE/GMS, and N-DE/GMS according to their origins, and the treated diatomite was named S-DE/GMS and J-DE/GMS according to its treatment method. All of the adsorption experiments in this work were repeated three times, and the average values were taken. The adsorption amount Qe (mg/g) was determined by the weight method and calculated as follows

$$Q_e = \frac{M_B - M_A}{M_A}$$

(1)

where M_A is the weight of the diatomite sample (g) and M_B is the total weight of the sample after adsorption (mg).

3. RESULTS AND DISCUSSION

3.1. Diatomite Samples Characteristics and Adsorption Properties. *3.1.1. Characteristics Analysis.* The XRD patterns of diatomite samples from the three origins are shown in Figure 2. As shown in Figure 2, the primary minerals found
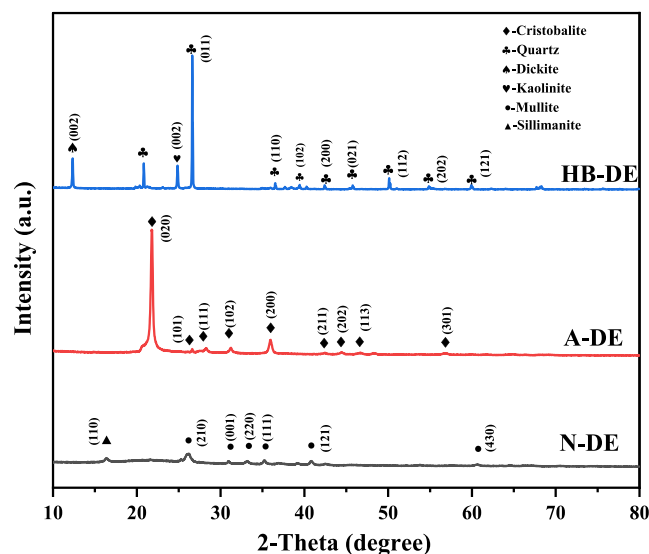

Figure 2. XRD patterns of diatomite samples from three origins.

in HB-DE samples were quartz and the associated minerals kaolinite and dickite. In the A-DE sample, the mineral composition was mainly square quartz transformed by high-temperature calcination of cristobalite with no other impurities.[27] Kaolinite in the N-DE sample was dehydroxylated and transformed into meta-kaolinite during calcination and then pyrolyzed into the quartz phase. When the temperature increased to 1200 °C, it led to mullite formation and the
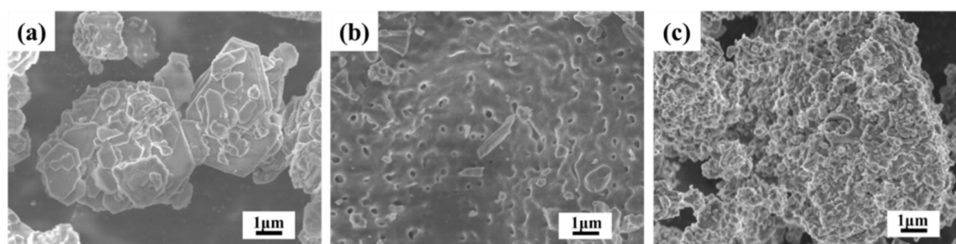
Figure 3. SEM images of diatomite samples from three origins: (a) HB-DE; (b) A-DE; (c) N-DE.

Table 1. Chemical Composition of Three Diatomite Samples (wt % Oxides) Measured by XRF

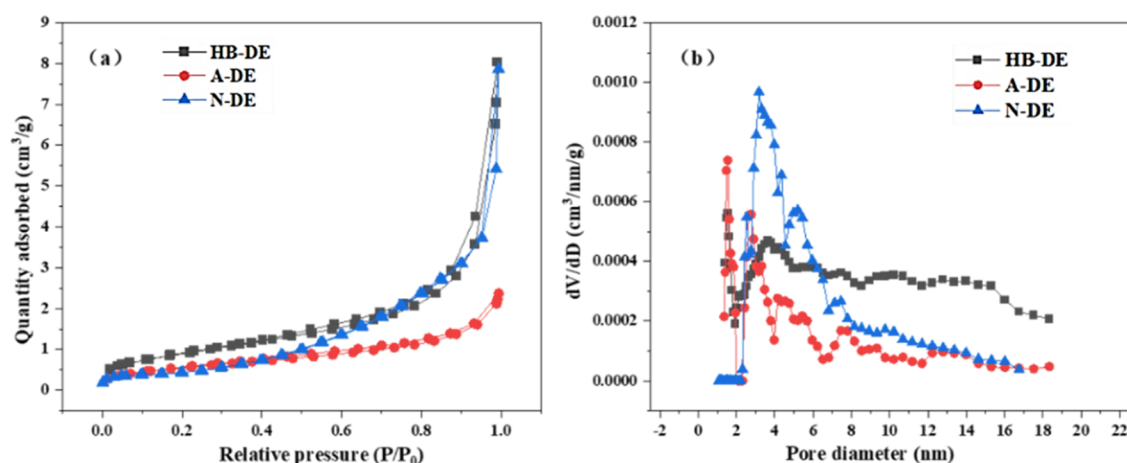| samples	SiO_2	Al_2O_3	Fe_2O_3	CaO	MgO	TiO_2	K_2O	Na_2O	other
HB-DE	73.30	25.60	0.24	0.10	0.03	0.29	0.13	0.01	0.30
A-DE	92.80	2.40	1.56	0.26	0.25	0.16	0.45	1.97	0.15
N-DE	50.80	46.70	0.45	0.16	0.07	1.34	0.15	0.05	0.28

Figure 4. (a) N_2 adsorption−desorption isotherms and (b) BJH pore size distributions of the diatomite samples from three origins.

pyrolysis of cristobalite. Then cristobalite started to transform into quartz melt and mullite content increased significantly at 1400−1500 °C.[28−30] In addition, a small amount of sillimanite would irreversibly form mullite under high-temperature calcination, as well. Thus, the main mineral composition in N-DE was quartz, mullite, and sillimanite.

The microscopic morphology of HB-DE, A-DE, and N-DE is shown in Figure 3. The irregular lamellae of various sizes were stacked together on the surface of the HB-DE sample (Figure 3a). The surface of the A-DE sample was arranged with multiple cylindrical pores of uneven pore size that were the main morphological feature present in the diatomite sample[31] and were favorable for storing the adsorbed small molecules. In addition, the surface or pore edge of this sample was partially covered by diatom fragments (Figure 3b), and the dense columnar and granular materials were present on the surface of the N-DE sample, aggregating with each other in a stacked state (Figure 3c).

As presented in Table 1, a compositional gap existed among the chemical compositions of three diatomite samples. The HB-DE sample had higher SiO_2 (73.30%) and Al_2O_3 (25.60%) contents. The A-DE sample had higher SiO_2 (92.80%), but lower Al_2O_3 (2.40%) contents. The N-DE sample had more average SiO_2 (50.80%) and Al_2O_3 (46.70%) contents. Nevertheless, Si and Al were the main elements in the three diatomite samples. The high amount of Si resulted from characteristic crystal structures such as quartz or cristobalite,

while the high content of Al resulted from clay minerals such as kaolinite and mullite. This suggested that clay was present in both the HB-DE and N-DE samples with the N-DE sample having a larger clay percentage. Every result matched the related XRD analysis quite well.

The N_2 adsorption−desorption isotherms and BJH pore size distributions of these three diatomite samples are shown in Figure 4a and b, respectively. According to the classification curves given by IUPAC, the N_2 adsorption−desorption isotherms of all three diatomite samples were type II, and there were obvious hysteresis loop structures in the relative pressure range of 0.2−0.9. As can be seen from Figure 4a, all of the diatomite samples had a small N_2 adsorption at a relative pressure of $P/P_0 < 0.1$, indicating that the microporous structure accounts for a smaller percentage in the three samples. The adsorption rate increased fast in the range of 0.2−0.9, indicating the existence of irregular mesoporous structures inside the diatomite and a larger proportion in the total pores. In Figure 4b, the pore sizes of the HB-DE sample were mainly distributed in the range of 0−20 nm, and the pore sizes of the A-DE sample were mostly distributed in the range of 0−6 nm, indicating that the micropores and mesoporous structures with small pore sizes were mainly present in HB-DE and A-DE samples. For the N-DE sample, the pore size was mainly distributed in the range of 2−8 nm, indicating that the mesopores mainly determined the size of the specific surface area in this sample. In addition, all diatomite samples showed a

decreasing trend in proportion as the pore size increased. As shown in Table 2, the specific surface area of the three

Table 2. Pore Structural Characteristics of Diatomite Samples from Three Origins

samples	BET surface area (m^2/g)	total pore volume (cm^3/g)	average pore diameter (nm)
HB-DE	3.298	0.012	15.112
A-DE	2.017	0.004	7.294
N-DE	1.564	0.012	31.148

diatomite samples was the largest for HB-DE, followed by A-DE, and the smallest for N-DE. The N-DE sample had some agglomeration, which caused the surface to create narrow pores. As a result, the average pore size of this sample was higher than that of the other samples.

3.1.2. Comparison of GMS Adsorption Properties. The adsorption properties of three origin diatomite samples for GMS at different concentrations are shown in Figure 5. Due to
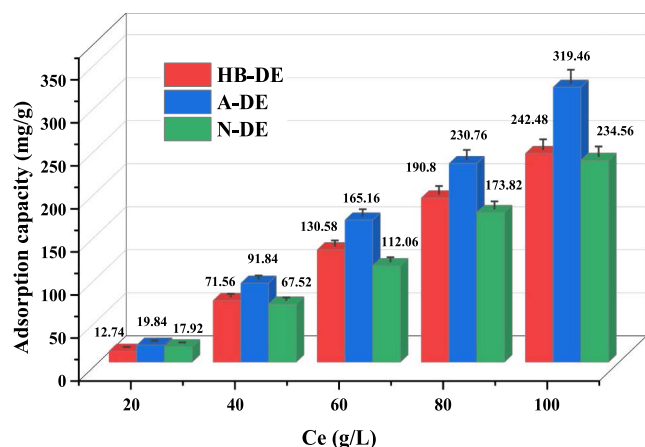

Figure 5. Comparison of the adsorption properties of three diatomite samples.

the inconsistent morphology and structure of diatomite from different producing areas, the adsorption performance of GMS was also different. As shown in Figure 5, under the same concentration conditions, the A-DE sample has the largest adsorption capacity, followed by N-DE, and HB-DE has the smallest. With increasing concentrations, the adsorption capacity of the three samples for GMS increased gradually. Under the maximum concentration of 100 g/L, the A-DE, HB-DE, and N-DE samples exhibited concentrations of 319.46, 242.48, and 234.56 mg/g, respectively. Therefore, the A-DE sample has the strongest adsorption capacity for GMS.

Analyzing the structure and adsorption capacity of three diatomite samples, the rich mesoporous structure in the diatomite structure was a factor that affected the adsorption capacity. However, the presence of associated minerals such as kaolinite in the HB-DE sample and the presence of mullite in the N-DE sample impeded the adsorption capacity of GMS.[32] After a comprehensive analysis was conducted, the A-DE sample was chosen as the mineral material before treatment. This decision was made to further enhance the adsorption capacity of diatomite for GMS and investigate the adsorption mechanism in greater detail. The adsorption properties for GMS were improved by increasing the number of surface

hydroxyl groups and expanding the specific surface area and pore size of micropores or mesopores.

3.2. Purification Diatomite Characteristics and Adsorption Properties. *3.2.1. Characteristics Analysis.* The XRD patterns of the A-DE, AS-DE, and AJ-DE samples are shown in Figure 6. As shown in Figure 6, the diffraction peaks
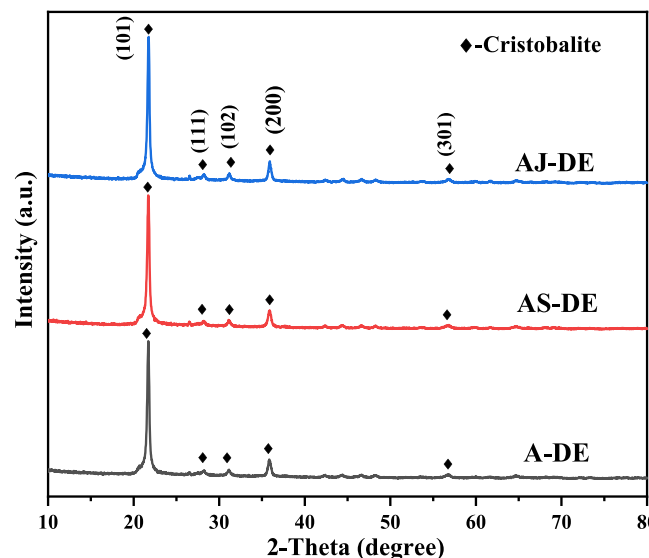

Figure 6. XRD patterns of diatomite samples before and after treatment.

shown in the plots of both AS-DE and AJ-DE samples were at $2\theta = 21.84$, 31.16, and 35.90°, which could be analyzed for (100), (102), and (200) crystal planes of cristobalite (JCPDS card no. 76-0940), indicating that the mineral composition of the samples after acid and alkali treatments were still cristobalite. The positions of their diffraction peaks were the same as those of the A-DE sample, indicating that both treatments do not affect the diatomite crystal structure.[33]

The FTIR spectra of diatomite samples before and after treatment are shown in Figure 7. For the A-DE sample, the
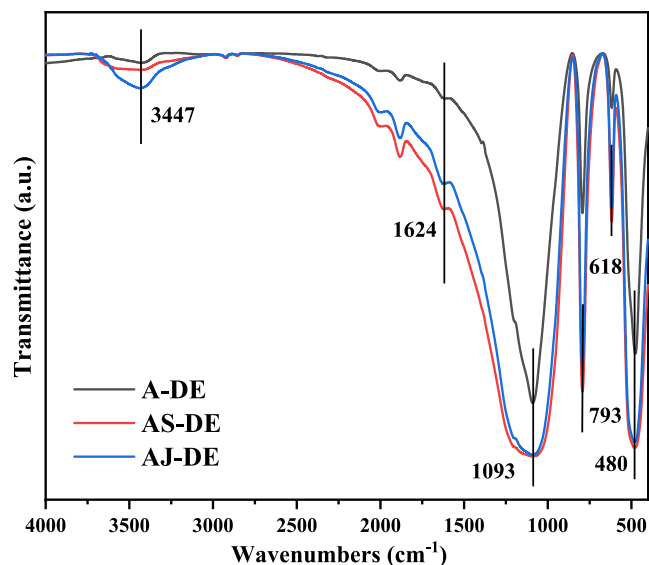

Figure 7. FTIR spectra of the diatomite samples before and after treatment.
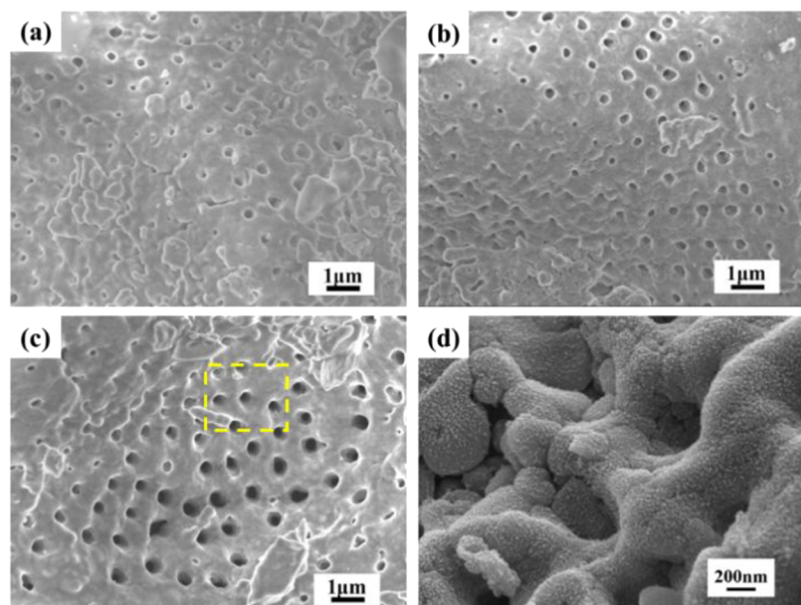
Figure 8. SEM images of diatomite samples before and after treatment: (a) A-DE; (b) AS-DE; (c) AJ-DE; (d) AJ-DE sample partial magnification.

bands at 1093 and 793 cm^{-1} were attributed to the asymmetric stretching vibration and symmetric stretching vibration of Si−O, respectively.[34] The tensile vibration peak of Si−O−Si was observed at 618 cm^{-1}, and the antisymmetric bending vibration peak of O−Si−O in silico-oxygen tetrahedron was 480 cm^{-1}, which were characteristic peaks of SiO_2 in diatomite particles.[35,36] The distinctive peak of Si−OH and adsorbed water on the diatomite particles was found at 3447 cm^{-1}, while the torsional vibration of Si−OH on the surface of the diatomite samples was responsible for the weak absorption peak at 1624 cm^{-1}.[37] The Si−OH on the diatomite surface was an important functional group, which could be divided into two types: one is isolated and the other is connected by a hydrogen bond, which made the diatomite surface appear weakly acidic.[38] Its presence provides active sites for absorption. Figure 7 shows that AS-DE and AJ-DE samples had significantly broadened hydroxyl vibrational peaks at 3100−3600 cm^{-1} compared to the A-DE sample. Additionally, the range of the surface −OH deformation vibrational peak at 1624 cm^{-1} was increased, indicating that both treatments increased the number of hydroxyl groups on the diatomite surface. Alkali treatment was more effective than acid treatment.

SEM images of diatomite before and after treatment are displayed in Figure 8, and the surface parameters are shown in Table 3. The pores on the surface sieve plate of the A-DE sample were relatively small and partially covered by some impurities on the surface (Figure 8a). After acid treatment, the originally covered impurities were removed from the surface pores of the AS-DE samples, exposing more clear pore

structures (Figure 8b), leading to an increase in pore volume and specific surface area[33] (Table 3). During the acid treatment process, the acid solution first formed a liquid film on the diatomite's surface. A portion of the acid molecules then diffused at the reaction interface, where they reacted with impurities in the skeleton's gaps before eventually entering the diatom's internal pores to react with internal oxide impurities. As seen in Figure 8c, the pore size on the surface of the AJ-DE sample was significantly larger and the pore edges were more rounded compared to those of A-DE and AS-DE. From the partial magnification of Figure 8c, it can be seen that a large number of nanoscale particles were uniformly encapsulated on the sample surface and inside the pores, which increased the roughness of the internal and external surfaces of diatomite (Figure 8d). This demonstrates that the diatomite structure can be entirely maintained by alkali treatment, even though the diatom fragments' pores, shell edges, and surface are eroded, etching a rich pore structure within the particles.[39,40] Additionally, they react with metal oxide impurities that are either inside or attached to the pore surface, increasing the specific surface area and pore size (Table 3).

The N_2 adsorption−desorption isotherms and BJH pore size distributions of the samples before and after treatment are shown in Figure 9a and b, respectively. As shown in Figure 9a, based on the classification curves given by IUPAC, the N_2 isothermal adsorption−desorption lines of all three samples are type II and there was an obvious hysteresis loop structure in the relative pressure range of 0.1−0.9, which indicates the presence of micropores and mesoporous structures in all three samples.[41] Compared to A-DE, the AS-DE sample showed an overall increase in N_2 adsorption in the relative pressure range of 0.1−1.0, indicating that acid treatment enhanced the pore structure of diatomite. AJ-DE sample had less adsorption in the low relative pressure region $(P/P_0 < 0.2)$ and stronger adsorption in the high relative pressure region $(P/P_0 > 0.8)$, indicating that after alkali treatment diatomite A-DE had a larger mesoporous structure inside. And as a whole, the adsorption of N_2 by A-DE, AS-DE, and AJ-DE was improved. As shown in Figure 9b, the pores with a size of about 2.5 nm

Table 3. Surface Parameters of Diatomite Samples before and after Treatment

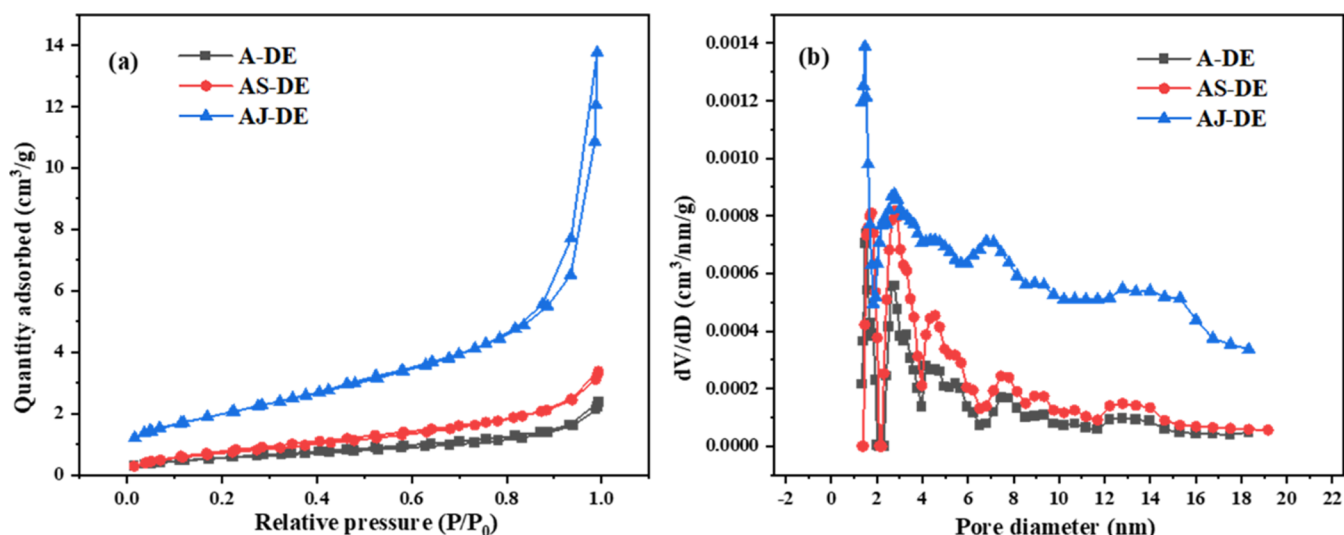| samples	BET surface area (m^2/g)	total pore volume (cm^3/g)	average pore diameter (nm)
A-DE	2.017	0.004	7.298
AS-DE	2.773	0.005	7.561
AJ-DE	7.253	0.021	11.767

Figure 9. (a) N_2 adsorption−desorption isotherms and (b) BJH pore size distributions of the diatomite samples before and after treatment.

accounted for the largest proportion of the A-DE samples, and most of the pores were distributed in the range of 2−4 nm. When the pore size continued to increase, the proportion of pores decreased gradually. After acid treatment, the pore sizes of the AS-DE sample were different, but most of them were still in the range of 2−4 nm, and the peak distribution was significantly enhanced in the range of 2−20 nm compared with that of A-DE. The peak distribution of pore size of the AJ-DE sample appeared in the range of 0−2 nm, which indicated that the alkali had a certain corrosive effect on the surface of diatomite, resulting in small-sized micropores on the surface. Compared with those of A-DE and AS-DE, the pore size distribution peaks of the AJ-DE sample were significantly more uniform. Combined with Table 3, it can be seen that the specific surface area, pore volume, and average pore size of AS-DE and AJ-DE samples increased compared to A-DE, in which the increase of the AJ-DE sample was more obvious.

3.2.2. Comparison of GMS Adsorption Properties. The adsorption capacity of diatomite samples on GMS before and after treatment is shown in Figure 10. It can be seen that the AS-DE and AJ-DE samples have a stronger adsorption capacity for GMS. At the concentration of 60 g/L, the adsorption of
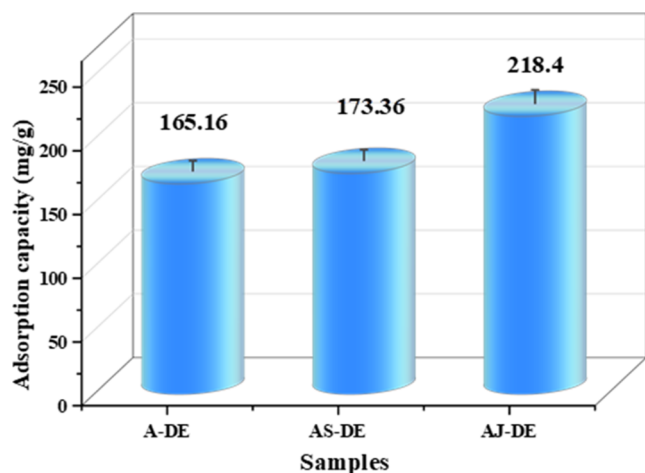
GMS could reach 218.14 mg/g for the AJ-DE sample and 173.36 mg/g for the AS-DE sample. Compared with the A-DE sample, the adsorption of the AJ-DE sample increased by 32.08% and the AS-DE sample increased by 6.78%. The results showed that the adsorption of GMS by alkali-treated diatomite was more significant and could be used as a treated method for diatomite before the preparation of mineral composites with high GMS content.

3.3. Adsorption Mechanism. The N_2 adsorption−desorption isotherms and BJH pore size distribution of AJ-DE/GMS composites are shown in Figure 11. As shown in
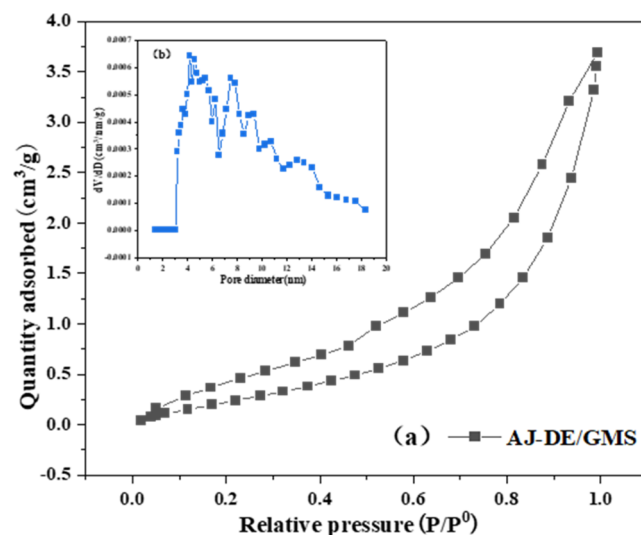

Figure 11. (a) N_2 adsorption−desorption isotherms and (b) the BJH pore diameter distribution of AJ-DE/GMS composites.

Figure 11a, the adsorption−desorption isotherms of AJ-DE/GMS composites were type II. The isothermal adsorption−desorption lines do not coincide in the low-pressure area, and the adsorption capacity was 0 when the pore size was distributed in the range of 0−2 nm (Figure 11b). Therefore, it can be inferred that part or all of the micropores of diatomite were blocked. The surface parameters of AJ-DE/GMS composites are summarized in Table 4. It can be seen from

Figure 10. Adsorption capacity of diatomite samples on GMS before and after treatment.

Table 4. Pore Structural Characteristics of the AJ-DE/GMS Composite Samples

samples	BET surface area (m^2/g)	total pore volume (cm^3/g)	average pore diameter (nm)
AJ-DE/GMS	1.172	0.006	19.574

Table 4 that the specific surface area of the composites after adsorption of GMS decreased, and the average pore diameter increased compared with that of AJ-DE. The reason may be that the diatomite particles adsorbed organic materials to each other and blocked the original pores. They then agglomerated to form new larger particles, and a slit formed between the large particles to increase the average pore size. Because of the slit that was formed, the pore volume did not increase but decreased, which also indicated that the micropores that existed in the diatomite were blocked, and absorbed part of the surfactant.[42]

The FITR spectra of GMS, AJ-DE, and AJ-DE/GMS samples are shown in Figure 12. As can be seen from Figure
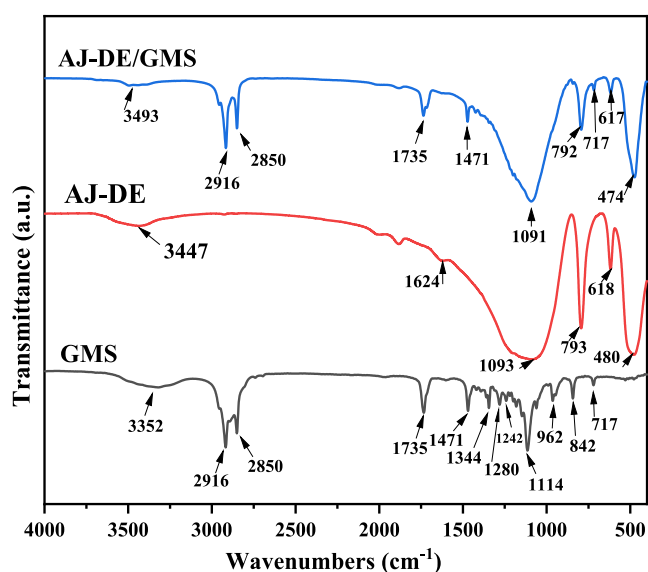
Figure 12. FTIR spectra of GMS, AJ-DE, and AJ-DE/GMS samples.

12, GMS all have characteristic peaks at 1471, 1244, 1280, 1242, 1114, 962, and 842 cm^{-1}, which proved that there was a long carbon chain fatty acid ester structure.[43] Compared with the AJ-DE sample, the AJ-DE/GMS composite showed the characteristic peaks of GMS at 1735, 1471, and 717 cm^{-1} after adsorption, and the characteristic peaks at 2916 and 2850 cm^{-1} were enhanced, confirming the composite effect of AJ-DE on some GMS molecules. In addition, the broad peak near 3500 cm^{-1} becomes smaller and the wavenumber increases, indicating that the free O−H bond stretching decreases, and the characteristic peak at 1624 cm^{-1} almost disappeared, speculating that the hydroxyl groups on the surface of diatomite may be desorbed from the water bound to the GMS molecules by hydrogen bonds and there is chemical adsorption.[44] However, since the main characteristic peaks of the GMS and AJ-DE samples were still present in the spectra of the AJ-DE/GMS composites, it was evidenced that the adsorption of AJ-DE samples on GMS was dominated by physical adsorption.

The SEM images of diatomite before and after adsorption, corresponding C element mapping diagram, and EDS graphs are shown in Figure 13. As shown in Figure 13a,b, the GMS molecules were not observed to aggregate on the pore surface in the samples obtained after adsorption; therefore, it was presumed that they entered the pore. By comparing the mapping of the C element before and after adsorption (Figure 13c,d), it can be found that the C element was evenly distributed on the surface of diatomite before adsorption, but there were more elements in the positions of pores after adsorption, which can also confirm the multilayer adsorption of droplet molecules on the surface of diatomite and fill the pores of the structure.[31] This finding was supported by our previous nitrogen adsorption experiment and BET analysis, showing the changes in surface area from 2.017 to 1.172 m^2/g after adsorption. In addition, EDS analysis before and after adsorption showed that the change of the carbon peak increased significantly, which verified the successful adsorption (Figure 13e,f).

According to the analysis presented above, diatomite can work well with polar GMS because it is a polar adsorbent. Furthermore, diatomite's excellent adsorption performance on GMS is largely due to the structure and surface characteristics of its micropores and mesopores. The micropore structure in diatomite was filled by the adsorption of GMS molecules through van der Waals forces, while the effect of mesopores on the adsorption properties was more significant than that of micropores. The specific surface area of diatomite was mostly determined by its mesoporous structure, which made up a greater percentage of its pores. It can increase the number of adsorption sites on the surface of diatomite and the probability of being adsorbed by collision with GMS molecules in comparison to micropores. The mesoporous structure in the adsorption−desorption process could act as a channel for diffusion and a storage area for several GMS molecules. The roughness of the inner pore wall and the inhomogeneity of this pore structure were two significant factors influencing the adsorption−desorption performance. Furthermore, the more expansive mesoporous structure could hold two or more layers of adsorbed mass, and capillary coalescence could happen when there was residual volume on both sides of the pore wall following adsorption, enhancing diatomite's adsorption ability. The diatomite also had a large number of hydroxyl groups on the pore surface, which could be adsorbed with oxygen in GMS in the form of hydrogen bonds.[45]

The mechanism diagram for the adsorption of nonionic surfactant GMS by diatomite is shown in Figure 14. GMS molecules collide with the surface of diatomite and are adsorbed there to undergo monolayer adsorption under specific adsorption conditions. The van der Waals force is the primary intermolecular force between the two. As the adsorption proceeds, diatomite forms multilayer adsorption inside and on both sides of the pore wall by acting as a hydrogen bonding agent and van der Waals force on the recollision GMS molecules. As the adsorption time increases, diatomite pores may be further adsorbed. The pores are then blocked by the GMS solution and the meniscus forms. This causes capillary condensation and additional GMS molecules to be adsorbed into the solution.[46,47]

Thus, the adsorption process of diatomite and GMS can be described as physical adsorption generated by uneven intermolecular tensions on both surfaces dominating as well as chemical adsorption that partially generates hydrogen
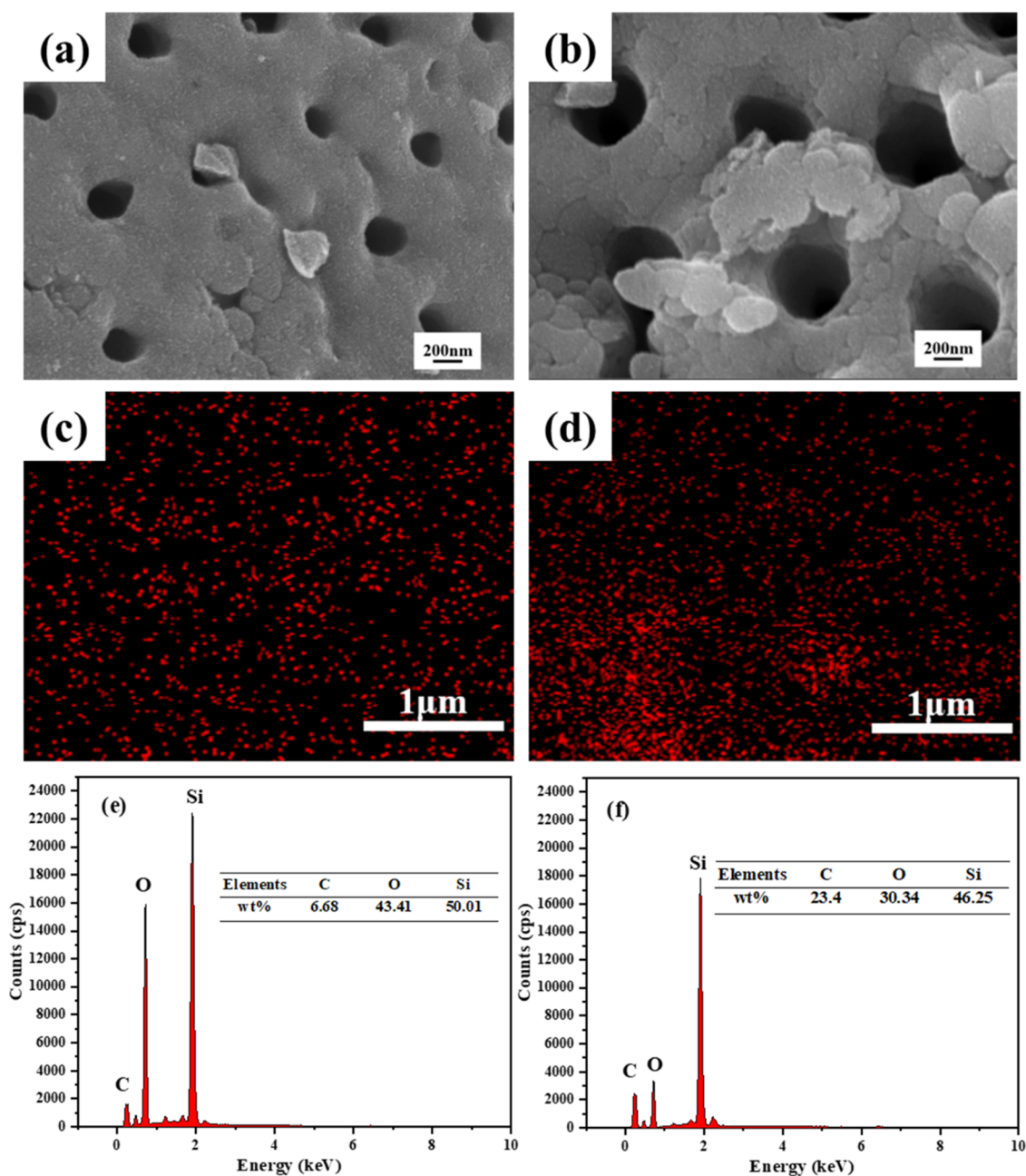
Figure 13. SEM images of (a) AJ-DE and (b)AJ-DE/GMS. C element mapping of (c) AJ-DE and (d) AJ-DE/GMS. EDS analysis of (e) AJ-DE and (f) AJ-DE/GMS.

bonds. Among these, chemical adsorption was more stable and tended to stay inside the diatomite, making it difficult to be desorbed. This suggests that GMS adsorbed by diatomite can achieve a slow release through partial desorption. On the other hand, physical adsorption was reversible in response to changes in external conditions.

3.4. Dripping Performance of the Film. The surface activity and diffusivity of the dripping agent were necessary to achieve a good wettability of the film. A comparison between the prepared LLDPE/LDPE-DE/GMS (L1) film and the LLDPE/LDPE-GMS (L0) film with the addition of simply GMS as a dripping agent was conducted to better portray the slow-release effect of the minerals. The contact angles of L0 and L1 films are shown in Figure 15. The L1 film had a 38° contact angle, which was smaller than that of the L0 film. The

addition of GMS significantly reduced the contact angle of the LLDPE film due to the strong hydrophilicity of the −OH groups of GMS.[48] In addition, according to Wenzel's correction to Young's equation, the surface was hydrophilic if the contact angle was less than 90°. At this time, the increase of film surface roughness will enhance the resistance caused by the multistage gradient diffusion of water droplets, it could reduce the contact angle with the film, and the surface was more hydrophilic.[49] Therefore, adding mineral DE/GMS to the inner, middle, and outer layers of the L1 film will increase the surface roughness. As each segment of the film possesses polar groups, the level of accumulation of GMS on the surface will increase gradually. Favorable hydrophilic properties facilitate the diffusion of water droplets on the film's surface,
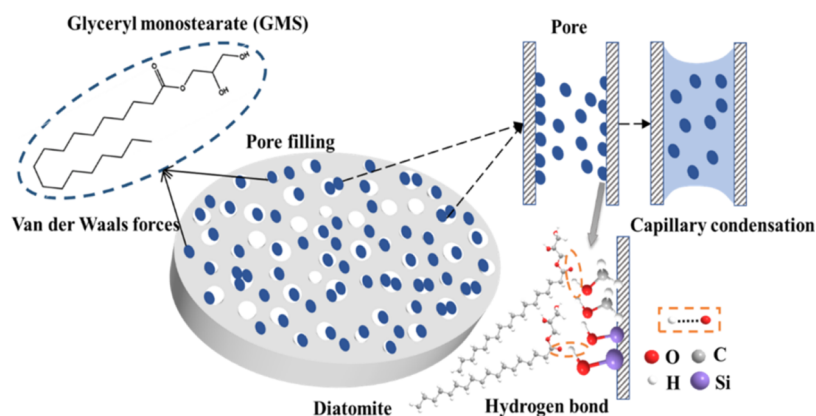
Figure 14. Mechanism diagram for the adsorption of the nonionic surfactant GMS by diatomite.
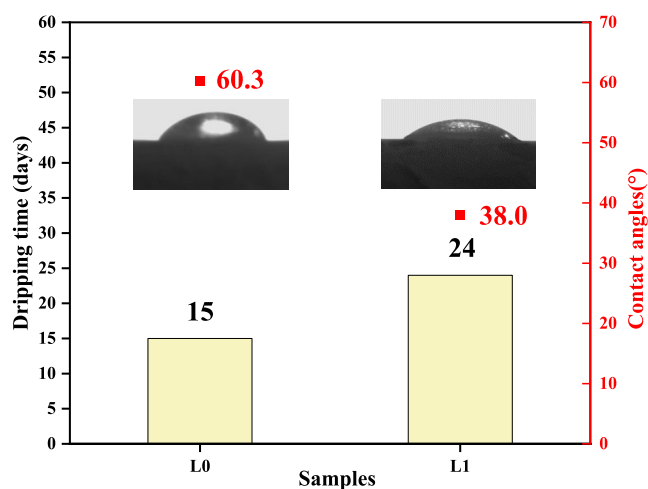

Figure 15. Comparison of the dripping performance of the L0 and L1 films.

consequently decreasing the water contact angle and enhancing wettability.

The dripping durations of L0 and L1 films are shown in Figure 15. As can be seen from the graph, the dripping duration of both L0 and L1 films was greater than 8 days, which meets the requirements of the GB/T4455−2019 national standard. After adding the inner, middle, and outer layers of the DE/GMS composite material to the prepared L1 film, the longest dripping durations could reach 24 days, which was 9 days longer than the L0 film. Evidently, the GMS adsorbed on diatomite could further prolong the dripping duration of the film. According to the literature, the dripping duration of 8 days in the accelerated drip method at 60 °C was equivalent to 3 months of field buckle film at room temperature.[50] Consequently, this computation indicated that the L1 film's dripping duration was equal to 9 months' worth of greenhouse field buckle film, which was sufficient to cover the majority of crops' greenhouse planting requirements. The results of this study showed that diatomite minerals can delay the precipitation of dripping agents, thereby extending the dripping durations.

4. CONCLUSIONS

Diatomite from the province of Jilin was chosen as the preferred mineral material for adding films after a comparison of its structural characteristics and ability to absorb GMS was

made. To further improve the adsorption capacity, the preferred samples were treated with acid and alkali in two ways, respectively. The results showed that both treatments did not affect the crystal structure of diatomite and were able to increase the number of hydroxyl groups and expand the pore volume. Compared with the sample before treatment, the adsorption of GMS by the alkali-treated sample could reach 218.14 mg/g, which increased by 32.08%, and the adsorption capacity of the acid-treated sample was 173.36 mg/g, which increased by 6.78%. The effect of alkali treatment on the samples was more significant than that of the acid treatment. The adsorption of glycerol monostearate on diatomite was mainly physical adsorption produced by an unbalanced van der Waals force, there was chemical adsorption by hydrogen bonding, and the process goes through three stages: monolayer adsorption, multimolecular layer adsorption, and capillary coalescence. In addition, according to the experimental data analysis, the dripping performance of the composite film was excellent. This work validates the adsorption relationship between minerals and dripping agents and the possibility of good properties for dripping films created using mineral composites, laying an experimental basis for further amplification studies and applications.

■ ASSOCIATED CONTENT

ⓢ Supporting Information

The Supporting Information is available free of charge at https://pubs.acs.org/doi/10.1021/acsomega.4c04308.

> Preparation method and required instrument of diatomite adsorption material; calculation of adsorption capacity of diatomite adsorbing glycerol monostearate; preparation method of DE/GMS composite material and the required instrument; preparation method of LLDPE/LDPE-DE/GMS material and the required instruments; and instruments used for some methods of characterization (PDF)

■ AUTHOR INFORMATION

Corresponding Authors

Hong Zhang − *Key Laboratory of Special Functional Materials for Ecological Environment and Information, Hebei University of Technology, Ministry of Education, Tianjin 300130, People's Republic of China; Institute of Power Source and Ecomaterials Science, School of Materials Science and Engineering, Hebei University of Technology, Tianjin*

300130, People's Republic of China; ⊚ orcid.org/0000-0001-9079-5203; Email: zhanghong@hebut.edu.cn

Jinsheng Liang − *Key Laboratory of Special Functional Materials for Ecological Environment and Information, Hebei University of Technology, Ministry of Education, Tianjin 300130, People's Republic of China; Institute of Power Source and Ecomaterials Science, School of Materials Science and Engineering, Hebei University of Technology, Tianjin 300130, People's Republic of China;* Email: liangjinsheng@hebut.edu.cn

Authors

Jindi Zha − *Key Laboratory of Special Functional Materials for Ecological Environment and Information, Hebei University of Technology, Ministry of Education, Tianjin 300130, People's Republic of China;* ⊚ orcid.org/0009-0001-8686-5325

Zhixiao Ren − *Key Laboratory of Special Functional Materials for Ecological Environment and Information, Hebei University of Technology, Ministry of Education, Tianjin 300130, People's Republic of China*

Na Zhang − *Key Laboratory of Special Functional Materials for Ecological Environment and Information, Hebei University of Technology, Ministry of Education, Tianjin 300130, People's Republic of China;* ⊚ orcid.org/0000-0002-2321-0014

Gengdi Zheng − *Beijing Lianfeixiang Technology Co., Ltd., Beijing 100011, People's Republic of China*

Wei Jin − *Beijing Lianfeixiang Technology Co., Ltd., Beijing 100011, People's Republic of China*

Complete contact information is available at:
https://pubs.acs.org/10.1021/acsomega.4c04308

Author Contributions

J.Z.: conceptualization, formal analysis, investigation, writing—original draft. H.Z.: writing—review and editing. Z.R.: investigation, validation, writing—review and editing. N.Z.: investigation, writing—review and editing. G.Z.: investigation, validation. W.J.: conceptualization, methodology, data curation. J.L.: conceptualization, resources, writing—review and editing, supervision, project administration, funding acquisition.

Notes

The authors declare no competing financial interest.

■ REFERENCES

(1) Touchaleaume, F.; Martin-Closas, L.; Angellier-Coussy, H.; Chevillard, A.; Cesar, G.; Gontard, N.; Gastaldi, E. Performance and environmental impact of biodegradable polymers as agricultural mulching films. *Chemosphere* 2016, 144, 433−439.

(2) Waldo-Mendoza, M. A.; Quinones-Jurado, Z. V.; Perez-Medina, J. C.; Yanez-Soto, B.; Ramirez-Gonzalez, P. E. Fogging Control on LDPE/EVA Coextruded Films: Wettability Behavior and Its Correlation with Electric Performance. *Membranes* 2017, 7 (1), 11.

(3) Whittingham, C. P. The chemical mechanism of photosynthesis. *Bot. Rev.* 1952, 18 (4), 245−290.

(4) Maechler, L.; Sarra-Bournet, C.; Chevallier, P.; Gherardi, N.; Laroche, G. Anti-Fog Layer Deposition onto Polymer Materials: A Multi-Step Approach. *Plasma Chem. Plasma Process.* 2011, 31 (1), 175−187.

(5) Sheng, Q.; Sun, J.; Wang, Q.; Wang, W.; Wang, H. S. On the onset of surface condensation: formation and transition mechanisms of condensation mode. *Sci. Rep.* 2016, 6 (1), No. 30764.

(6) Ren, S. C.; Wang, L.; Yu, H. J.; Haroon, M.; Ullah, R. S.; Haq, F.; Khan, R. U.; Fahad, S. Recent progress in synthesis of antifogging agents and their application to agricultural films: a review. *J. Coat. Technol. Res.* 2018, 15 (3), 445−455.

(7) Wei, J.; Luo, X.; Lin, X.; Zhang, H. Impact of Monoolein on the Anti-Fogging Property of Polyethylene Greenhouse Film. *Polym. Mater. Sci. Eng.* 2013, 29 (5), 71−73.

(8) Durán, I. R.; Laroche, G. Current trends, challenges, and perspectives of anti-fogging technology: Surface and material design, fabrication strategies, and beyond. *Prog. Mater. Sci.* 2019, 99, 106−186.

(9) Rosen-Kligvasser, J.; Suckeveriene, R. Y.; Tchoudakov, R.; Narkis, M. LLDPE films containing monoester of oleic acid grafted to silica particles as durable antifog additives. *Polym. Adv. Technol.* 2017, 28 (8), 931−939.

(10) Ming, C.; Jianfu, Z.; Lihang, Q.; et al. Preparation and Properties of Grafted Polyethylene/GMS Grafted Modified SiO2 Blends. *Chem. J. Chin. Univ.-Chin.* 2018, 39 (12), 2781−2788.

(11) Plasman, V.; Caulier, T.; Boulos, N. Polyglycerol esters demonstrate superior antifogging properties for films. *Plast. Addit. Compd.* 2005, 7 (2), 30−33.

(12) Irusta, L.; Gonzalez, A.; Fernandez-Berridi, M. J.; Iruin, J. J.; Asua, J. M.; Albizu, I.; Ibarzabal, A.; Salmeron, A.; Espi, E.; Fontecha, A.; Garcia, Y.; Real, A. I. Migration of Antifog Additives in Agricultural Films of Low-Density Polyethylene and Ethylene-Vinyl Acetate Copolymers. *J. Appl. Polym. Sci.* 2009, 111 (5), 2299−2307.

(13) Shlosman, K.; Rosen-Kligvasser, J.; Suckeveriene, R.; Tchoudakov, R.; Narkis, M. Novel antifog modification for controlled migration and prolonged wetting of LLDPE thin films. *Eur. Polym. J.* 2017, 90, 220−230.

(14) Li, W. F.; Yao, Z. H.; Yuan, Y.; Meng, Y.; Xie, L. Synthesis and Characterization of Linear Low Density Polyethylene Grafted Glycerol Monolauric Acid Monoitaconic Acid Diester. *Polym.-Plast. Technol. Eng.* 2012, 51 (6), 620−625.

(15) Rosen-Kligvasser, J.; Suckeveriene, R. Y.; Tchoudakov, R.; Narkis, M. A novel methodology for controlled migration of antifog from thin polyolefin films. *Polym. Eng. Sci.* 2014, 54, 2023−2028.

(16) Yang, S. Q.; Wang, H. Y.; Sun, X. P.; Yang, F. H.; Li, X. T.; Li, W. F.; Yao, Z. H. Synthesis of a dripping agent based on lauric acid diethanolamide and delaying its migration in LLDPE films. *Polym.-Plast. Technol. Mater.* 2020, 59 (10), 1100−1108.

(17) Zhu, D. T.; Wu, Q.; Li, W. F.; Yao, Z. H.Preparation and properties of kaolin grafted alkyl amine type dripping agent/polyethylene composites *Acta Mater. Compos. Sin.* 2020; Vol. 37 1, pp 35−41.

(18) Benkacem, T.; Hamdi, B.; Chamayou, A.; Balard, H.; Calvet, R. Physicochemical characterization of a diatomaceous upon an acid treatment: a focus on surface properties by inverse gas chromatography. *Powder Technol.* 2016, 294, 498−507.

(19) Jing, Y. N.; Jing, Z. Z.; Ishida, E. H. Relationship between porous and mechanical properties of hydrothermally synthesized porous materials from diatomaceous earth. *Ind. Eng. Chem. Res.* 2013, 52 (50), 17865−17870.

(20) Caliskan, N.; Kul, A. R.; Alkan, S.; Sogut, E. G.; Alacabey, I. Adsorption of Zinc(II) on diatomite and manganese-oxide-modified diatomite: A kinetic and equilibrium study. *J. Hazard. Mater.* 2011, 193, 27−36.

(21) Aw, M. S.; Simovic, S.; Yu, Y.; Addai-Mensah, J.; Losic, D. Porous silica microshells from diatoms as biocarrier for drug delivery applications. *Powder Technol.* 2012, 223, 52−58.

(22) Aivalioti, M.; Vamvasakis, I.; Gidarakos, E. BTEX and MTBE adsorption onto raw and thermally modified diatomite. *J. Hazard. Mater.* 2010, 178 (1−3), 136−143.

(23) He, W.; Fang, Q. H.; Lin, W.; Luyt, A. S.; Ge, T. J. Study on anti-fog films of polyethylene modified with inorganic micrometer diatomite. *Appl. Mech. Mater.* 2012, 200, 347−350.

(24) Jingmei, B.; Shucai, L.; Mingjuan, P. Effects of Auxiliary Agents on Properties of Polyethylene Antifogging Films *Plast. Sci. Technol.*, **2005**.

(25) Bariana, M.; Aw, M. S.; Kurkuri, M.; Losic, D. Tuning drug loading and release properties of diatom silica microparticles by surface modifications. *Int. J. Pharm.* **2013**, *443* (1−2), 230−241.

(26) Abu-Zurayk, R. A.; Al Bakain, R. Z.; Hamadneh, I.; Al-Dujaili, A. H. Adsorption of Pb(II), Cr(III) and Cr(VI) from aqueous solution by surfactant-modified diatomaceous earth: Equilibrium, kinetic and thermodynamic modeling studies. *Int. J. Miner. Process.* **2015**, *140*, 79−87.

(27) Manevich, V. E.; Subbotin, R. K.; Nikiforov, E. A.; Senik, N. A.; Meshkov, A. V. Diatomite - siliceous material for the glass industry. *Glass Ceram.* **2012**, *69* (5−6), 168−172.

(28) He, H. P.; Guo, J. G.; Zhu, J. X.; Yuan, P.; Hu, C. Si-29 and Al-27 MAS NMR spectra of mullites from different kaolinites. *Spectrochim. Acta, Part A* **2004**, *60* (5), 1061−1064.

(29) Lv, S. Y.; Ma, A. Q.; Li, H.; Gao, Y. Q.Preparation of mullite ceramics from coal gangue *J. Mater. Sci. Eng.* 2022; Vol. *40* 1, pp 104−109.

(30) Yuan, W. Q.; Kuang, J. Z.; Huang, Z. Y.; Yu, M. M. Effect of aluminum source on the kinetics and mechanism of mullite preparation from kaolinite. *Chem. Phys. Lett.* **2022**, *787*, 139242 DOI: 10.1016/j.cplett.2021.139242.

(31) Aw, M. S.; Simovic, S.; Addai-Mensah, J.; Losic, D. Silica microcapsules from diatoms as new carrier for delivery of therapeutics. *Nanomedicine* **2011**, *6* (7), 1159−1173.

(32) Salloum, M. J.; Dudas, M. J.; Mcgill, W. B.; Murphy, S. M. Surfactant sorption to soil and geologic samples with varying mineralogical and chemical properties. *Environ. Toxicol. Chem.* **2000**, *19* (10), 2436−2442.

(33) Chaisena, A.; Rangsriwatananon, K. Synthesis of sodium zeolites from natural and modified diatomite. *Mater. Lett.* **2005**, *59* (12), 1474−1479.

(34) Huang, Y. N.; Jiang, Z. M.; Schwieger, W. Vibrational spectroscopic studies of layered silicates. *Chem. Mater.* **1999**, *11* (5), 1210−1217, DOI: 10.1021/cm980403m.

(35) Padmanabhan, S. K.; Pal, S.; Ulhaq, E.; Licciulli, A. Nanocrystalline TiO2−diatomite composite catalysts: effect of crystallization on the photocatalytic degradation of rhodamine B. *Appl. Catal., A* **2014**, *485*, 157−162.

(36) Jingshen, D.; Liu, Q. J. Research on the coagulant aid effects of modified diatomite on coal microbial flocculation. *Water Sci. Technol.* **2019**, *80* (10), 1893−1901.

(37) Mu, Q. Y.; Wang, Y. D. Synthesis, characterization, shape-preserved transformation, and optical properties of La(OH)(3), La2O2CO3, and La2O3 nanorods. *J. Alloys Compd.* **2011**, *509* (2), 396−401.

(38) Zhao, Y.; Tian, G. Y.; Duan, X. H.; Liang, X. H.; Meng, J. P.; Liang, J. S. Environmental applications of diatomite minerals in removing heavy metals from water. *Ind. Eng. Chem. Res.* **2019**, *58* (27), 11638−11652.

(39) Tsai, W. T.; Hsien, K. J.; Yang, J. M. Silica adsorbent prepared from spent diatomaceous earth and its application to removal of dye from aqueous solution. *J. Colloid Interface Sci.* **2004**, *275* (2), 428−433.

(40) Gago, C.; Romar, A.; Fernandez-Marcos, M.; Álvarez-Rodríguez, E. Fluoride sorption and desorption on soils located in the surroundings of an aluminium smelter in Galicia (NW Spain). *Environ. Earth Sci.* **2014**, *72*, 4105−4114.

(41) Rouquerol, J.; Rouquerol, F.; Sing, K. *Adsorption by Powders and Porous Solids, Principles, Methodology and Applications*; Academic Press, 1999.

(42) Sekulić, D. R.; Babić, B. M.; Kljajević, L. M.; Stašić, J. M.; Kaluđerović, B. V. The effect of gamma radiation on the properties of activated carbon cloth. *J. Serb. Chem. Soc.* **2009**, *74* (10), 1125−1132.

(43) Kato, T.; Nakamura, T.; Yamashita, M.; Kawaguchi, M.; Kato, T.; Itoh, T. Surfactant properties of purified polyglycerol mono-laurates. *J. Surfactants Deterg.* **2003**, *6*, 331−337.

(44) Chen, J. F.; Zhang, W. Y.; Li, X. Preparation and characterization of konjac glucomannan-acrylic acid-diatomite composites. *Polym. Compos.* **2016**, *37* (12), 3384−3390.

(45) Yuan, P.; Wu, D. Q.; He, H. P.; Lin, Z. Y. The hydroxyl species and acid sites on diatomite surface: a combined IR and Raman study. *Appl. Surf. Sci.* **2004**, *227* (1−4), 30−39.

(46) Ma, S. C.; Wang, Z. G.; Zhang, J. L.; Sun, D. H.; Liu, G. X. Detection analysis of surface hydroxyl active sites and simulation calculation of the surface dissociation constants of aqueous diatomite suspensions. *Appl. Surf. Sci.* **2015**, *327*, 453−461.

(47) Liu, D.; Yu, W. B.; Deng, L. L.; Yuan, W. W.; Ma, L. Y.; Yuan, P.; Du, P. X.; He, H. P. Possible mechanism of structural incorporation of Al into diatomite during the deposition process I. Via a condensation reaction of hydroxyl groups. *J. Colloid Interface Sci.* **2016**, *461*, 64−68.

(48) Yang, S. Q.; Zhu, D. T.; Yang, F. H.; Li, W. F.; Yao, Z. H.; Liu, B. W. An effective method for delayed migration of dripping agent from linear low-density polyethylene films. *Polym. Adv. Technol.* **2021**, *32* (4), 1560−1567.

(49) Wenzel, R. N. Resistance of solid surfaces to wetting by water. *Ind. Eng. Chem.* **1936**, *28* (8), 988−994.

(50) Zheng, W. W.; Xu, X. F.; Gou, Y. K.; Zhu, T. X.; Cai, W. L.; Huang, J. Y.; Lai, Y. K. Rational construction of multifunctional hydrophilic coatings with sustainable anti-fogging, UV-shielding and anti-freezing abilities. *Chem. Eng. J.* **2023**, *459*, No. 141605.